RSC Advances

PAPER

View Article Online
View Journal | View Issue

Cite this: *RSC Adv.*, 2016, **6**, 78219

Simultaneous Cu doping and growth of TiO_2 nanocrystalline array film as a glucose biosensor†

Yunyu Cai,[a] Yixing Ye,[a] Shouliang Wu,[a] Jun Liu[a] and Changhao Liang*[ab]

Received 9th June 2016
Accepted 12th August 2016

DOI: 10.1039/c6ra15014d

www.rsc.org/advances

Doping additional ions into a semiconductor is a potential strategy to modify the electronic structure of semiconductor materials. By using highly reactive colloidal Cu clusters as doping precursor, we present here the successful doping of Cu ions into a TiO_2 nanocrystalline material that simultaneously transformed from amorphous anodic TiO_2 nanotubes through a dissolution and recrystallization process. The Cu-doped TiO_2 nanoparticle (Cu-TNP) film was characterized by X-ray diffraction, scanning and transmission electron microscopy and Raman spectroscopy. The Cu-TNPs show a rugby-like shape with exposed active {101} and {001} facets and the long-axis parallel to the [001] lattice direction. The substitutional Cu^{2+} ion dopants in the TiO_2 nanocrystals caused the swelling of the crystalline unit cell. Such an efficient doping design facilitates the improvement of nanostructured TiO_2 as a potential biosensor for glucose molecules.

Introduction

Titanium dioxide (TiO_2) is an important biomaterial for application in biomedical fields such as for bone reconstruction, intravascular stents, drug delivery and biosensing.[1] Since Cosnier and coworkers reported that mesoporous TiO_2 films could work as a glucose biosensor by immobilizing enzyme molecules under an amperometric approach in 1997,[2] various nanostructured TiO_2 materials combined with glucose oxidase have been used in the fabrication of sensitive and stable biosensors. Although the sensitivity and stability can be further improved by designing new nanostructures and/or loading new chemical substances,[1] the difficulties from immobilizing enzymes, storing at low temperature, prolonging validity and lowering the cost of the device are still troublesome. So, it has attracted great endeavor to substitute economical and durable inorganic electrochemical catalysts (metals, alloys and metal oxides) for fragile enzymes because these active materials could directly catalyze the electrochemical oxidization of glucose molecules in alkaline media. For example, Yu *et al.*, proved that TiO_2 nanotubes decorated with Ni nanoparticles (NPs) can display high catalytic electroactivity for the oxidation of glucose with the detection limit of 2 μM.[3] Li *et al.*, enhanced the sensitivity to 1590.9 μA mM^{-1} cm^{-2} by loading Ni–Cu alloy NPs on TiO_2 nanotubes.[4] Luo *et al.*, reported that CuO nanofibers modified TiO_2 nanotubes in glucose sensing was of a low sensitivity of 79.79 μA mM^{-1} cm^{-2}, but a good detection limit of 1 μM.[5]

Noted that in the sensor application, the real active catalytic centers are the oxidized species of catalytic metal, which are usually oxidized before sensing and function as active electron-transfer mediators after absorbing glucose molecules.[6] The metal decorated TiO_2 usually suffers multiple cyclic voltammetry (CV) sweeping in strong alkali solution to incite increasing number of oxidized species as active sites for metal catalysis. However, this pre-treatment step compels the erosion of TiO_2 in strong alkali solution. Herein, directly combining the metal oxide with TiO_2 is desirable for fast and simple sensing detection in practical application. On the other hand, the electrode needs an extra polymer binder (such as Nafion) to immobilize TiO_2 sensor. It may reduce catalytic active sites and then degrade the glucose sensitivity, meanwhile the inevitable separation of the TiO_2 sensor from the electrode after persistent operation can lead to loss in electrochemical activity.[4] Moreover, preparation of specimens *via* chemical approaches could introduce contaminations from other chemicals, which would impair the biocompatibility of TiO_2 in sensing process.[7] Therefore, an alternative and green approach to combine oxidized species of catalytic metal with TiO_2 that fixed or *in situ* grown on the conductive substrate is thus desirable.

[a]*Key Laboratory of Materials Physics and Anhui Key Laboratory of Nanomaterials and Nanotechnology, Institute of Solid State Physics, Chinese Academy of Sciences, Hefei 230031, China. E-mail: chliang@issp.ac.cn*

[b]*Department of Materials Science and Engineering, University of Science and Technology of China, Hefei 230026, China*

† Electronic supplementary information (ESI) available: Eqn (S1) for deducing the change in unit cell parameters (*a*, *b*, *c*) of tetragonal-system compounds; Fig. S1 SEM image, TEM image, XRD pattern of Cu colloid nanoparticles; Fig. S2 EDX spectrum of Cu-TNPs and the table of corresponding elements calculation; Fig. S3 Ti K-edge EXAFS spectra and Cu K-edge EXAFS spectra of different specimens through k^3-weighted Fourier transform; Fig. S4 minus Nyquist plots of as-synthesized Cu-TNPs and anatase TNTs products from EIS measurements; Fig. S5 CV curves of Cu-TNPs in 0.1 M NaOH solution with different scan rates and relationship between response currents and scan rates; Fig. S6 amperometric responses of the Cu-TNPs to different interfering species. See DOI: 10.1039/c6ra15014d

Doping is an effective way to introduce metallic ions or oxidized species into compounds. There are various methods such as sol–gel,[8] magnetron sputtering,[9] and solution impregnation,[10] proposed for doping in TiO_2 for photocatalysis and biosensor. However, achieving green and uniform doping in TiO_2 crystalline lattice and simultaneously immobilizing the as-formed doped composite on a fixed substrate remains a great challenge. Particularly for doping in nanoscale crystals, the self-purification effect of nanoscale crystalline even results in segregation or accumulation of impurities on surfaces or grain boundaries.[11,12] Many reports have proved that TiO_2 nanotubes (TNTs) array film could be *in situ* anodized on Ti substrate to form a Schottky-type contact that benefit the rapid transport of electrons to Ti substrate in biosensing process.[4] An appropriate and green doping strategy to get uniform distribution of impurities in TiO_2 array structure together with immobilized Ti substrate is favor for practical sensor application.

Laser ablation in liquids (LAL) is a powerful technique to obtain high purity nanocrystals with unique physicochemical properties.[13–16] LAL employs the high temperatures and high pressure characteristics in laser-induced plasma plume, which lead to unsaturated valences and defects on the surface of the resulted nanocrystals because of the nonequilibrium growth processes.[15] Here, to use the array structure of TNTs as an immobilized substrate, we intentionally select LAL-derived reactive Cu colloid as the precursor of dopants. We demonstrated the efficiency of *in situ* doping of Cu^{2+} ions in TiO_2 in a dissolution–recrystallization process under hydrothermal treatment. The Cu^{2+} ions dopants in anatase nanocrystals increased the swelling of crystal unit cell.

Experimental

Preparation of TNTs by anodic oxidation of Ti

A 0.25 mm thick Ti foil (99.99%) was sequentially cleaned in acetone, ethyl alcohol, and water under sonication, and then dried in air at room temperature. All of the chemical solvents and reagents are analytical grade. The anodizing electrolyte is ethylene glycol solvent containing 0.25 wt% NH_4F and 2 vol% H_2O. One side of the metal Ti foil contacted with the electrolyte through a 15 cm diameter O-ring. Graphite was used as the counter electrode in a two-electrode cell. Anodic oxidation was conducted at room temperature for 90 min at a DC voltage of 60 V. After repeated washing with deionized water and drying, some pieces of the as-formed TNTs films were annealed at 450 °C for 2 h for the subsequent comparative experiments and some films were kept amorphous for hydrothermal procedure.

Hydrothermal treatment of LAL-derived Cu colloid and TNTs film

Colloidal Cu solution was prepared by LAL technique (Fig. S1 in ESI†). Briefly, a Cu target (99.99%) was immobilized on a supporter in a vessel filled with 15 mL deionized water. The Cu target was then irradiated for 10 min by an Nd/YAG pulsed laser with 1064 nm wavelength, 10 Hz frequency, 10 ns pulse duration, and 100 mJ per pulse energy. The fresh colloid (15 mL) was sealed in an autoclave containing a piece of amorphous TNTs film. The hydrothermal reaction proceeded for 15 h at 200 °C. After the reaction, the film was obtained and repeatedly washed in deionized water, and finally dried for further investigations.

Structural characterization and properties of Cu-doped TiO_2 NP film

An FEI Sirion 200 field-emission scanning electron microscopy (FESEM) was used to evaluate the morphology of the film product. The crystalline structure was investigated on high-resolution transmission electron microscopy (HRTEM) (JEM, JEOL-2010). In TEM sample preparation, small amount of the product was stripped from the Ti metal substrate and then ultrasonically dispersed in ethanol, and the obtained suspensions were then dropped onto a holey-carbon coated molybdenum-grid. The phase structure was investigated by using X-ray diffraction (XRD) with the use of a Philips diffractometer (X'pert Pro) with Cu-Kα radiation ($\lambda = 1.5419$ Å). Electrochemical CV spectra, amperometric curves, and impedance spectra curves of the Cu-doped TiO_2 nanoparticles (Cu-TNPs) and blank anatase TNTs were obtained through a Zahner IM6e Electrochemical Workstation to investigate the response as nonenzymatic glucose biosensors. Zeta potential of the Cu colloid was measured by a Zetasizer 3000 HSa.

The structural features of Cu-TNPs and annealed anatase TNTs without hydrothermal treatment were further analyzed through X-ray absorption fine structure (XAFS) spectrometer, including X-ray absorption near-edge structure (XANES) and extended X-ray absorption fine structure (EXAFS). The XAFS spectra for Cu-K edge of the Cu-TNPs and Ti-K edge of the two anatase TNTs samples (sample annealed at 450 °C and hydrothermally treated sample) were obtained by using beamline BL14W1, belonging to Shanghai synchrotron radiation, administrated by Shanghai Institute of Applied Physics (Shanghai, China). Transmission (standard Cu foil, Cu_2O, and CuO) and fluorescence yield (Cu-TNPs and TNTs) spectra were obtained with the use of a double-crystal Si (111) monochromator, ion chambers, and a Ge solid-state detector equipped with Ni filter. The XAFS data were analyzed through an Athena program. Cu foil, Cu_2O, and CuO were used to extract the experimental XANES features of the Cu metal, Cu^+, and Cu^{2+} ions, respectively.

Results and discussion

Fig. 1a and b show the top and side view images (inserted plot) of the anodized TNTs before and after hydrothermal-treatment. The original TNTs-like shape disappeared and only the NPs accumulated which was depicted as a Cu-TNPs film array on the Ti substrate. Fig. 1b shows the compact assembly array of those NPs, with an average particle size of <100 nm standing on the upper surface of Cu-TNPs film. Seeing from the inserted plot in Fig. 1b, the NPs accumulated one by one along the direction of the original TNTs. The original thickness of TNTs array film was

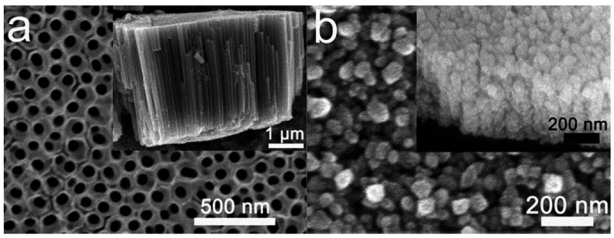

Fig. 1 Top and side views (inserted plot) of the amorphous TNTs (a) and Cu doped-TNPs (b).

about 4.6 μm, and it was changed to about 400 nm after hydrothermal process.

HRTEM investigation provides more detailed structure and phase information. Fig. 2a shows a single particle in a rugby-like shape. The partial zone in the white rectangle was magnified in Fig. 2b and the corresponding selected area electron diffraction (SAED) pattern is shown in Fig. 2c. The lattice spacings of 4.74 and 3.53 Å correspond to (002) and (101) crystalline planes of the anatase TiO_2, the angle between the two planes (68.3°) is consistent with the standard data. The crystals grew along the long-axis of ellipsoid that is parallel to [001] lattice direction with the exposed active {100} and {101} facets. Corresponding to the assembled NPs in Fig. 2d, the elemental mapping images in Fig. 2e–g display the dispersion of O, Ti, and Cu, respectively, in the accumulated NPs. The amount of Cu was significantly lesser than the other two elements. The result of energy-dispersive X-ray spectroscopy shows that the atomic weight percentages of Ti and Cu were respectively 16.35 and 0.4 (Fig. S2 in ESI†).

The XRD pattern shows the composition and structural information of the products. For comparison, TNTs samples were also annealed at 450 °C for 2 h to form pure anatase phase. The XRD results (Fig. 3) indicated no significant difference between the anatase TNTs (red curve) and the Cu-TNPs (blue curve). All of the peaks are consistent with the data of standard cards [JCPDS card no. 21-1272 (anatase TiO_2) and JCPDS card

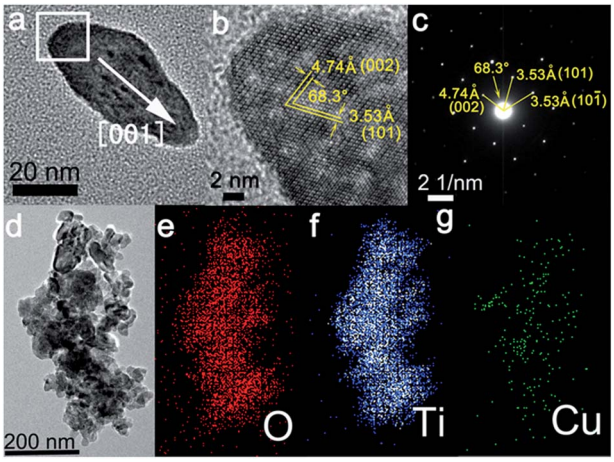

Fig. 2 (a) TEM image of a single Cu-TNPs; (b) magnified image of NP in (a); (c) corresponding SAED pattern of NP in (b); and (d) TEM image of accumulated NPs. (e–g) Elemental mapping images of O, Ti, and Cu corresponding to that in (d).

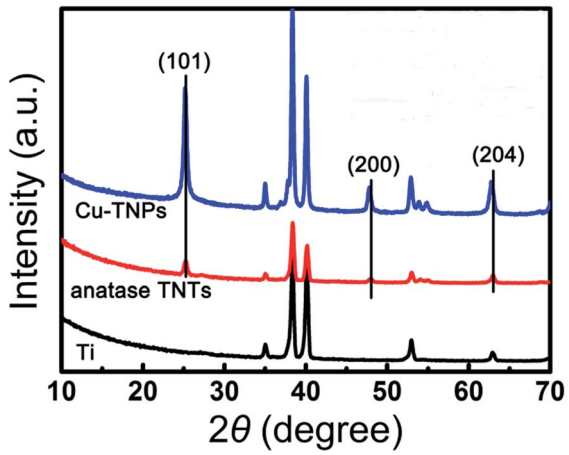

Fig. 3 XRD patterns of Cu-TNPs, anatase TNTs, and metal Ti foil.

no. 44-1294 (hexagonal Ti)]. The observed phases were consistent with the HRTEM analysis. However, three peaks at 25.4° (101), 48.0° (200), and 63.0° (204) of the anatase TNTs film a little shifted to the low-angle direction, thereby leading to the increase in *d*-spacings of (101), (200), and (204) planes from 3.520, 1.892, and 1.480 Å to 3.532, 1.901 and 1.487 Å, respectively. According to eqn (S1) in ESI† for tetragonal-system compounds, the change in unit cell parameters (*a*, *b*, *c*) could be deduced. In this study, the *a* and *c* values increased from 3.785 and 9.513 Å to 3.803 and 9.543 Å in the anatase structure. The distortion of anatase lattice could be due to the doping of Cu species in the inner sites of original lattices.

Fig. 4 shows the Raman spectra of the annealed TNTs (black curve) and Cu-TNPs (red curve). The four typical Raman peaks of the anatase phase were found at 147 cm^{-1} (E_g mode), 399 cm^{-1} (B_{1g} mode), 517 cm^{-1} (both A_{1g} and B_{1g} modes), and 637 cm^{-1} (E_g mode) for the TNTs sample.[17] The dominant phase of Cu-TNPs is also the anatase TiO_2 structure as XRD results. Similar to many reports about introducing metal ions into TiO_2 lattice by substitutional strategy,[18,19] Raman active modes of Cu-TNPs slightly shifted to lower frequency zone, respectively at

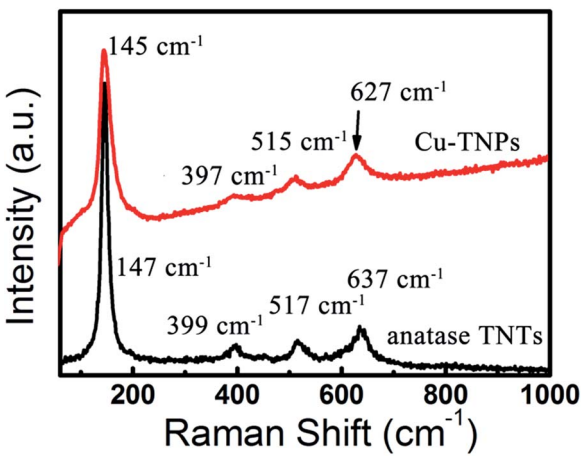

Fig. 4 Raman spectra of Cu-TNPs and anatase TNTs.

145 cm^{-1}, 397 cm^{-1}, 515 cm^{-1} and 627 cm^{-1}. Based on the extensive energetic computation results, it was especially easier for transition metals to substitute Ti sites than to form interstitial defects.[20] Here, we proposed that the shift of Raman peaks was due to the enlargement of anatase lattice by substitutional doping of Cu ions.

Fig. 5a shows the Cu K-edge XAFS spectra of the Cu foil, Cu_2O, CuO, and the as-prepared Cu-TNPs, and Fig. 5b shows the corresponding XANES spectra of these samples at the pre-edge region. In the XAFS spectrum, it is obvious to find that the dominant main peak and the shoulder peaks at the post-edge region of the Cu-TNPs most resembled those of CuO. In the XANES spectra, the pre-edge peaks were always intrinsic for various Cu ions species.[21] The characteristic peaks of the Cu^{2+} ions were found at (i) approximately 8976 eV to 8979 eV (a very weak absorption caused by the dipole-forbidden 1s → 3d electronic transition), and (ii) at approximately 8985 eV to 8988 eV as a shoulder peak, as well as at approximately 8995 eV to 8998 eV as an intense peak (both attributed to the 1s → 4p transition). The Cu^{+} ions are normally discriminated by a single peak at 8983 eV to 8984 eV. In Fig. 5b, peak A at 8978 eV and peak B at 8986 eV were observed for CuO, whereas the peaks C and D were found at 8983 and 8982 eV, respectively, which correspond to the pre-edge absorption of Cu^{+} ions in Cu_2O and Cu atoms in the Cu foil. For the Cu-TNPs, the weak pre-edge absorption at 8978 eV (peak A) and the intense peak between 8995 eV and 8998 eV both belong to Cu^{2+} ions were found. However, the pre-edge shoulder peak B wasn't observed probably due to the low concentration of dopants. Therefore, the oxidation state of the Cu species in the Cu-TNPs sample was Cu^{2+} ions. The post-edge region of the XAFS spectrum (EXAFS) could be presented in energy space, such as in Fig. 5a and b. EXAFS could also be shown in wave-vector space (k space) with the use of k^3-weighted Fourier transform in Athena programs. Fig. S3a in ESI† shows the EXAFS spectra of the Ti K-edge absorption of the annealed TNT sample without hydrothermal treatment and the Cu-TNPs sample, while Fig. S3b† compares the Cu K-edge EXAFS spectra of Cu foil, Cu_2O, CuO and Cu-TNPs in k-space. The Ti K-edge curves for the annealed TNTs (black) and the Cu-TNPs (red) were almost the same. Therefore, the coordination environments have no significant variation for the Ti^{4+} ions in the anatase TiO_2 with and without hydrothermal treatment. For the Cu-TNPs Cu K-edge in Fig. S3b,† the oscillation trend in the k-space apparently departed from the other three curves of Cu foil, Cu_2O, CuO, respectively. This phenomenon further proved that the coordination circumstances of the dopants in anatase lattice varied with Cu species in metal Cu or oxides. We could thus assume that the dopants did not change the anatase lattice environment largely, which was consistent with the above data analysis.

Fig. 6 was the general schematic view of the formation of Cu TNPs array film from TNTs array film with a simultaneous doping process. Amorphous TNTs could dissolve *in situ* as TiO_6 octahedral unit in water under hydrothermal conditions and then recrystallize as anatase NPs, which are inclined to deposit at the undissolved surfaces of TNTs.[22,26] These NPs accumulate along the direction of original array after absolute dissolution of the TNT film. For the anatase phase of TiO_2, each octahedral TiO_6 unit is connected with other four units by edge-sharing and with another four by corner-sharing. In addition, the surface of TiO_6 was negatively charged because of the surplus of O^{2-} ions, whereas the zeta potential of the as-formed colloid was approximately +23.5 mV, thereby indicating that the surfaces of LAL-generated colloidal Cu clusters were positively charged. The electrostatic attraction results in Cu doping during the recrystallization process. As substitutional dopants in the lattice, Cu^{2+} ions can occupy the site of Ti^{4+} ions in TiO_6 octahedrons.[23] Although less bonding of the substitutional species with the nearest O^{2-} ions could not be neglected totally, the major role of larger Cu^{2+} ions was to swell the unit cell in accordance with the enlarged a and c lattice parameters according to XRD, Raman and XAFS analysis.

Cu is famous in oxidizing carbohydrate without surface poisoning in biosensing.[24] Glucose is a typical biosensing target because it is essential to organisms, and electrochemical technology is a popular technique for biosensing assessment. All of the tests were conducted with the use of saturated Ag/AgCl as the reference electrode and Pt foil as the counter electrode. Both the anatase TNTs and the Cu-TNPs were used as working electrodes and sealed with the use of an epoxy resin, leaving an exposed area of 7 cm^2 on the top surface. Fig. 7a shows the CV sweeps of the two samples in 0.1 M NaOH aqueous solutions with and without 10 mM glucose solute. The sweeping at 50 mV s^{-1} was from 0 V to +0.8 V and then back to 0 V. Curves A and B, which are for the anatase TNTs, are close to rectangles and did

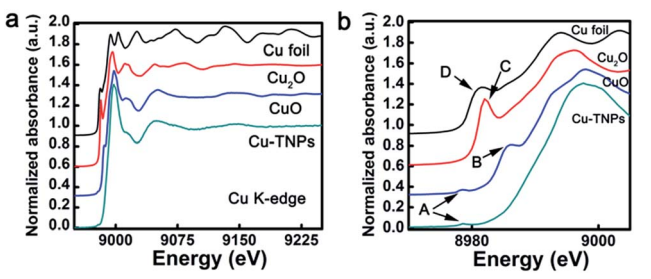

Fig. 5 (a) XAFS spectra of Cu foil, Cu_2O, CuO, and Cu-TNPs; (b) XANES spectra of Cu foil, Cu_2O, CuO, and Cu-TNPs in (a).

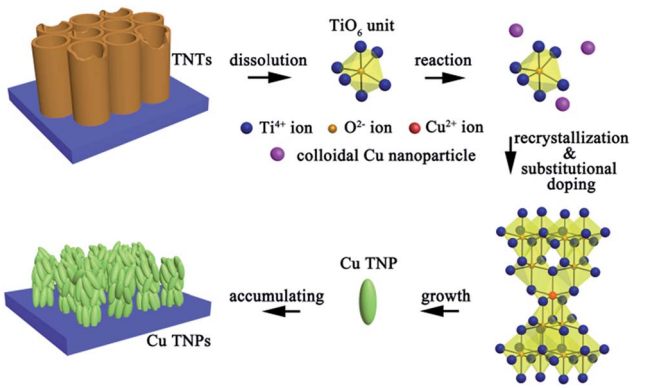

Fig. 6 Schematic illustration of formation of Cu TNPs array film.

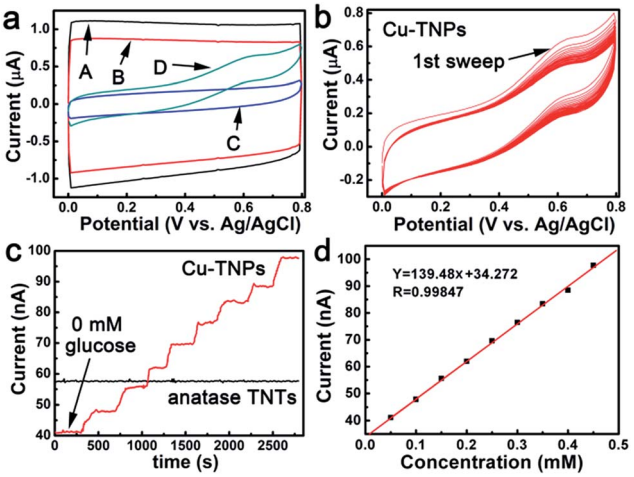

Fig. 7 (a) CV sweeping of anatase TNTs in 0.1 M NaOH solution (curve A) and in 0.1 M NaOH solution with 10 mM glucose (curve B); Cu-TNPs in 0.1 M NaOH solution (curve C) and in 0.1 M NaOH solution with 10 mM glucose (curve D). (b) 30 times CV sweeping of Cu-TNPs in 0.1 M NaOH solution with 10 mM glucose. (c) Amperometric response of Cu-TNPs and anatase TNTs at +0.65 V with successive addition of 7.5 μL glucose solution (100 mM) at 5 min intervals in 15 mL NaOH solution (0.1 M). (d) Linear relationship between the oxidation current of Cu-TNPs and glucose concentration.

not show any response triggered by the absorbed molecules on the surface of the electrode. Curve C also did not display any oxidation or reduction peaks. Only curve D showed an apparent current response at approximately +0.65 V, which was attributed to the oxidation peak of glucose on active Cu^{2+}/Cu^{3+} electron-transfer mediators.[25]

The reaction processes[6] are described with the use of eqn (1)–(3). Without pre-oxidation of the electrode, the Cu^{2+} ions in the TiO_2 NPs could directly function as active sites for glucose oxidation. The 30 successive sweeps in NaOH solution with glucose (Fig. 7b) confirmed that the doped electrode was stable under CV. Fig. 7c shows the amperometric responses of the anatase TNTs and the Cu-TNPs with added 7.5 μL pure glucose aqueous solution (100 mM) at 5 min intervals in 15 mL NaOH solution (0.1 M) under +0.65 V oxidation potential. No significant current response was found for the anatase TNTs, whereas the current increased significantly at each addition of glucose for the Cu-TNPs. The initial current response of the anatase TNTs was higher than that of Cu-TNPs, which is possibly due to the enhanced interfacial impedance of the accumulation NPs (Fig. S4, see ESI†). Fig. 7d shows the linear relationship between the response current of Cu-TNPs and the concentration of glucose in NaOH solution. This relationship directly reflected the fast and stable sensor behaviours of Cu-TNPs in response to glucose molecules. In order to estimate the kinetics of Cu-TNPs electrode, the CV curves (in Fig. S5(a)†) of the specimen measured in 0.1 M NaOH solution at different scan rates (from 10 mV s^{-1} to 150 mV s^{-1}) were tested. The response currents were read at + 0.65 V. Fig. S5(b)† shows the nearly linear relationship between the response currents and the square roots of scan rates. It indicated that the electrocatalytic process on the surface of Cu-TNPs was in diffusion controlled. According to the standard deviation derived from Fig. 7d, the detection limit of glucose was found to be about 40 μM. In Fig. S6,† selectivity of the Cu-TNPs was studied by adding interfering species during Amperometric response test. Ascorbic acid, fructose and uric acid were selected as interfering molecules. It showed that the Cu-TNPs electrode could sensitively discriminate glucose molecules, but could not obviously response to the interfering molecules.

$$Cu^{2+} \rightarrow Cu^{3+} + e^{-} \quad (1)$$

$$Cu^{3+} + \text{glucose} \rightarrow Cu^{2+} + \text{intermediate} \quad (2)$$

$$Cu^{3+} + \text{intermediate} \rightarrow Cu^{2+} + \text{product} \quad (3)$$

Conclusions

In summary, we developed an efficient doping and *in situ* phase modification route to obtain Cu-doped TiO_2 nanocrystalline film by hydrothermal treatment with the use of anodic TNTs and LAL-derived colloidal Cu clusters as precursors. The Cu-doped anatase NPs accumulated one by one along the original direction of the initial amorphous TNTs, thereby resulting in a new TiO_2 NPs film on the immobilized Ti substrate. The unique array morphology was observed even after TNTs dissolution and *in situ* phase transition from amorphous TiO_2 to rugby-shaped single-crystal TiO_2 NPs with preferred [001] long-axis growth direction and exposed active {001}, {101} facets. The substitutional Cu dopants in the anatase nanocrystals caused the swelling of crystal unit cell. The film showed an excellent biosensing performance in the electrochemical test with the use of glucose molecules as targets. The present experimental design for fabricating doped-TiO_2 NPs film on immobilized substrate could be extended to the construction of similar structures for device in other applications.

Acknowledgements

This work was financial supported by the National Basic Research Program of China (2014CB931704), the National Natural Science Foundation of China (NSFC, No. 51371166, 51571186, 11404338, 11304315, 51401206, 11504375) and China Postdoctoral Science Foundation.

References

1 S. L. Wu, Z. Y. Weng, X. M. Liu, K. W. K. Yeung and P. K. Chu, *Adv. Funct. Mater.*, 2014, **35**, 5464.
2 S. Cosnier, C. Gondran, A. Senillou, M. Gratzel and N. Vlachopoulos, *Electroanalysis*, 1997, **9**, 1387.
3 S. J. Yu, X. Peng, G. Z. Cao, M. Zhou, L. Qiao, J. Y. Yao and H. C. He, *Electrochim. Acta*, 2012, **76**, 512.
4 X. L. Li, J. Y. Yao, F. L. Liu, H. C. He, M. Zhou, N. Mao, P. Xiao and Y. H. Zhang, *Sens. Actuators, B*, 2013, **181**, 501.

5 S. Luo, F. Su, C. Liu, J. Li, R. Liu, Y. Xiao, Y. Li, X. Liu and Q. Cai, *Talanta*, 2011, **86**, 157.
6 I. Danaee, M. Jafarian, F. Forouzandeh, F. Gobal and M. G. Mahjani, *Electrochim. Acta*, 2008, **53**, 6602.
7 R. Sabetrasekh, H. Tiainen, J. E. Reseland, J. Will, J. E. Ellingsen, S. P. Lyngstadaas and H. J. Haugen, *Biomed. Mater.*, 2010, **5**, 015003.
8 G. Colón, M. Maicu, M. C. Hidalgo and J. A. Navío, *Appl. Catal., B*, 2006, **67**, 41.
9 W. Zhang, Y. Li, S. Zhu and F. Wang, *Catal. Today*, 2004, **93–95**, 589.
10 K. Lalitha, G. Sadanandam, V. D. Kumari, M. Subrahmanyam, B. Sreedhar and N. Y. Hebalkar, *J. Phys. Chem. C*, 2010, **114**, 22181.
11 G. M. Dalpian and J. R. Chelikowsky, *Phys. Rev. Lett.*, 2006, **96**, 226802.
12 D. Mocatta, G. Cohen, J. Schattner, O. Millo, E. Rabani and U. Banin, *Science*, 2011, **332**, 77.
13 C. Liang, Z. Tian, T. Tsuruoka, W. Cai and N. Koshizaki, *J. Photochem. Photobiol., A*, 2011, **224**, 110.
14 G. Yang, *Prog. Mater. Sci.*, 2007, **52**, 648.
15 J. Liu, C. Liang, Z. Tian, S. Zhang and G. Shao, *Sci. Rep.*, 2013, **3**, 1741.
16 J. Yang, T. Ling, W. T. Wu, H. Liu, M. R. Gao, C. Ling, L. Li and X. W. Du, *Nat. Commun.*, 2013, **4**, 1695.
17 C. Liang, K. Terabe, T. Hasegawa and M. Aono, *Appl. Phys. Express*, 2008, **1**, 064002.
18 Z. Y. Zhang, C. L. Shao, L. N. Zhang and X. H. Li, *J. Colloid Interface Sci.*, 2010, **351**, 57.
19 B. Santara, B. Pal and P. K. Giri, *J. Appl. Phys.*, 2011, **110**, 114322.
20 K. N. Song, X. P. Han and G. S. Shao, *J. Alloys Compd.*, 2013, **551**, 118.
21 H. Irie, K. Kamiya, T. Shibanuma, S. Miura, D. A. Tryk, T. Yokoyama and K. Hashimoto, *J. Phys. Chem. C*, 2009, **113**, 10761.
22 K. Huo, H. Wang, X. Zhang, Y. Cao and P. K. Chu, *ChemPlusChem*, 2012, **77**, 323.
23 J. U. Brehm, M. Winterer and H. Hahn, *J. Appl. Phys.*, 2006, **100**, 064311.
24 M. M. Rahman, A. J. Ahammad, J. H. Jin, S. J. Ahn and J. J. Lee, *Sensors*, 2010, **10**, 4855.
25 S. Luo, F. Su, C. Liu, J. Li, R. Liu, Y. Xiao, Y. Li, X. Liu and Q. Cai, *Talanta*, 2011, **86**, 157.
26 J. M. Wu, S. Hayakawa, K. Tsuru and A. Osaka, *J. Am. Ceram. Soc.*, 2004, **87**, 1635.